Investigation of surfactant effect on the bubble shape and mass transfer in a milli-channel using high-resolution microfocus X-ray imaging

Haghnegahdar, M.; Boden, S.; Hampel, U.;

Originally published:

September 2016

International Journal of Multiphase Flow 87(2016), 184-196

DOI: https://doi.org/10.1016/j.ijmultiphaseflow.2016.09.010

Perma-Link to Publication Repository of HZDR:

https://www.hzdr.de/publications/Publ-23948

Investigation of surfactant effect on the bubble shape and mass transfer in a milli-channel using high-resolution microfocus X-ray imaging

Mohammadreza Haghnegahdar[a] (corresponding author)

[a] Institute of Fluid Dynamics, Helmholtz-Zentrum Dresden - Rossendorf, Bautzner Landstr. 400, 01328 Dresden, Germany. Phone: +49 351 260 3767, Fax: +49 351 260 2383, Email: m.haghnegahdar@hzdr.de

Stephan Boden[a]

[a] Institute of Fluid Dynamics, Helmholtz-Zentrum Dresden - Rossendorf, Bautzner Landstr. 400, 01328 Dresden, Germany. Phone: +49 351 260 3773, Fax: +49 351 260 2383, Email: s.boden@hzdr.de

Uwe Hampel[a,b]

[a] Institute of Fluid Dynamics, Helmholtz-Zentrum Dresden - Rossendorf, Bautzner Landstr. 400, 01328 Dresden, Germany.

[b] AREVA Endowed Chair of Imaging Techniques in Energy and Process Engineering, Technische Universität Dresden, 01062 Dresden, Germany.

Phone: +49 351 260 3460, Fax: +49 351 260 1 2772, Email: u.hampel@hzdr.de

Investigation of surfactant effect on the bubble shape and mass transfer in a milli-channel using high-resolution microfocus X-ray imaging

Abstract

In this paper we present an experimental study on the influence of surface active agents (surfactants) on Taylor bubble flow in a vertical millimeter-size channel. Moreover we give a short review on the subject and previous investigations. We investigated the shape and dissolution rate of individual elongated carbon dioxide Taylor bubbles, which were hydraulically fixed in a downward flow of water. Bubble shape and dissolution rate was determined from microfocus X-ray radiographs. From the shrinking rate we calculated the liquid side mass transfer coefficient.

The results show that the presence of surfactants causes a change of the bubble shape and leads to a slight increase of the liquid film thickness around the bubble and as a result the elongation of contaminated bubbles. In addition, the comparison of clean and contaminated bubbles indicate that presence of surfactant has a more significant impact on the dissolution rate of small bubbles. Furthermore, applying different concentrations of surfactant reveals that in our case, where surface coverage ratio of surfactant on the bubbles is high, increase of contamination does not have a noticeable influence on the mass transfer coefficient of bubbles.

Keywords: Surfactant; Film thickness; Mass transfer; Taylor bubble; Carbon dioxide; Milli-channels

1 Introduction

Monolith froth reactors and millimeter-sized reactors have gained a great research interest from the industry and academia because of their advantages such as large interfacial area, high mass transfer rates, low pressure drop, and ease of scale-up over the conventional reactor technology [1]. To improve the efficiency of this kind of reactors, it is required to understand the relationship between the mass transfer rate and other important parameters. For gas-liquid two-phase systems, one of the main factors, which is known to have a significant influence both on the hydrodynamics and mass transfer

rate of phases, is presence of surface active agents (surfactants). Surfactants are adsorbed at gas–liquid interfaces and decrease the surface tension. The presence of surfactants in multiphase systems, either in the form of unavoidable impurities or as additives, has a great effect on the shape and the dynamics of the interfaces [2]. Great attention has been paid to investigate the effect of surfactants on small and/or spherical bubbles in infinite liquid both theoretically and experimentally, while contamination of large/elongated bubbles in small channels are subject of only few studies. In the following, the most relevant studies on the effect of surfactants on the gas-liquid systems are shortly reviewed.

1.1 Theoretical investigations

Regarding theoretical studies, Weber [3] investigated the effect of surfactant on the mass transfer of spherical-cap bubbles at Reynolds number ($Re=\rho D U_b/\mu$) higher than 100, where U_b is bubble rise velocity, D the channel diameter, ρ the liquid density and μ the liquid dynamic viscosity. It was supposed that the surfactant forms a stagnant film on the spherical surface near the rim of the bubble and its effect was attributed to a balance between surface forces and shear forces. Comparison of their results with experimental data showed agreement within 25%. Stokes flow due to the motion of a liquid drop or bubble in a contaminated immiscible fluid was analyzed by Sadhal and Johnson [4]. An exact solution was found for the resulting problem for an arbitrary cap angle and an expression for the drag force in terms of viscosities and the cap angle was for the first time developed. The dissolution of spherical bubbles at low Reynolds numbers was studied by Dani [5] using Direct Numerical Simulation (DNS) for fully contaminated, partially contaminated and clean bubbles by applying the conventional stagnant cap model. The comparison of results with classical relations showed the good scaling of Sherwood number ($Sh=Dk_L/D_c$) with $Pe^{1/3}$ and $Re^{1/2}$ respectively for solid sphere and clean bubble in creeping flow, where Pe ($=DU_b/D_c$) is Peclet number, k_L the liquid side mass transfer coefficient and D_c the gas molecular diffusion coefficient.

In a comprehensive study, Muradoglu and Tryggvason [6] developed a finite-difference/front-tracking method to simulate the interfacial flows with soluble surfactants. In their method both the interface and bulk surfactant concentration evolution equations were solved and coupled with the incompressible flow equations. The simulation was done to predict the influence of surfactant on the

hydrodynamics of buoyant viscous bubbles in a straight channel. It was found that the contaminated bubble behaves like a solid sphere in the limit of very low Reynolds number $Re < 1$ and the results were found to be in a good agreement with the experimental correlations collected by Clift et al. [7]. Tasoglu et al. [8] used the same approach to study the unsteady motion and deformation of a bubble rising in an otherwise quiescent liquid. They showed that the surfactant generally decreases the terminal velocity of the bubble but this reduction is most noticeable in the nearly spherical regime in which the bubble behaves like a solid sphere and its terminal velocity reaches that of a solid sphere.

Cuenot et al. [9] considered the similar problem and confirmed the validity of the well-known stagnant-cap model for describing the flow around a bubble contaminated by surfactants. Their results indicated a considerable rise of the drag which in several cases reaches the value corresponding to a rigid sphere. Hayashi and Tomiyama [10] investigated the effect of surfactant on the terminal velocity of Taylor bubbles in vertical pipes. They applied an interface tracking method and simulated for various Eötvös numbers ($Eo=\Delta\rho g D^2/\sigma$), different surfactant concentration and two different surfactants, where g is acceleration by gravity, σ surface tension and $\Delta\rho$ the density difference between two phases. They showed that the terminal velocity of bubbles increased because of reduction of surface tension near the bubble nose and since the bubbles at high Eötvös numbers are independent of surface tension, the presence of surfactant does not affect the terminal velocities of high Eötvös number bubbles.

Ghadiali and Gaver [11] utilized a numerical model of semi-infinite air bubbles in a capillary to analyze the continual interfacial expansion dynamics that occur during the opening of collapsed pulmonary airways. They showed that the surfactant properties can strongly affect the interfacial pressure drop through modification of the surface tension and the creation of Marangoni effect. In addition, they showed that, depending upon the range of parameters, either film thickening or film thinning responses are possible.

In case of liquid film thickness around the bubble, Ginley and Radke [12] presented a regular perturbation expansion in large adsorption rates within the low capillary number, singular perturbation hydrodynamic theory of Bretherton. They considered surface transport of the surfactants and neglected all concentration gradients in the bulk phase and showed that by addition of soluble surfactant to the

liquid phase, the surface concentration increases in the thin film region and leads to a decrease in the film thickness compared to the surfactant-free case. In contrary, in a more comprehensive analysis and for a semi-infinite bubble in a capillary, Ratulowski and Chang [13] carried out an asymptotic analysis for various convective, diffusive and kinetic timescales and showed that, if transport in the film is mass-transfer limited, the film thickness increases by a maximum factor of $4^{2/3}$ over Bretherton's mobile result at low bubble speeds. Stebe and Barthes-Biesel [14] considered the same problem for a viscous surfactant solution at high concentration. They considered the case where the surfactant flux is adsorption-desorption controlled and the equations of momentum and mass transfer are coupled to leading order. The results showed that interfaces with surface viscosities require larger pressure drops to aspirate the flow and leave thicker wetting layers along the capillary walls. For finite length bubbles in capillaries, Park [15] studied the influence of soluble surfactant on the steady motion of inviscid bubbles. Both front and rear ends of the bubble were examined in the limit of small capillary number and it was shown that due to the accumulation of the surfactant at the rear end of the bubble, the film thickening effect of the surfactant occurs only when the bubble length is greater than a certain critical value.

Daripa and Pasa [16] presented a theoretical proof for the thickening phenomenon in Bretherton problem applying perturbation theory and a lubrication analysis of the flow equations in a horizontal capillary. In another work [17], they investigated the influence of surfactant in a vertical capillary tube containing a viscous fluid and sealed at one end. They only considered interfacial surfactant on the interface of bubbles and ignored the presence of surfactant in the bulk. However, they showed that the presence of surfactant on the bubble interface gives a thinning effect on the thickness of the liquid layer behind the bubble. Recently, Olgac and Muradoglu [18] considered the impact of both insoluble and soluble surfactants on the motion of long bubbles in horizontal axisymmetric capillaries computationally using a finite-difference method. The results showed that both the insoluble and soluble surfactant have a thickening effect on the film thickness, which is especially prominent at low capillary numbers, Ca ($=\frac{\mu U_b}{\sigma}$).

1.2 Experimental investigations

In case of experimental studies, Mancy and Okun [19] studied the various factors involved in the influence of surfactant on the rate of oxygen dissolution in aeration process. They used Aerosol O.T. as surfactant and showed that addition of small amounts of Aerosol O.T. causes to reduction of oxygen transfer to a minimum. Griffith [20] investigated the impact of surfactants on the terminal velocity of bubbles and drops. They showed that terminal velocity at small Reynolds numbers are related to the cap size and then to the type and amount of surfactant. Using high speed photography technique, Raymond and Zieminski [21] studied the influence of aliphatic alcohols on mass transfer and drag coefficients of a single carbon dioxide bubble. The results showed that the concentration, molecular size, and structure of the investigated alcohols have a great effect on mass transfer as well as drag coefficients of the rising bubble. In a stirred tank, Vazquez et al. [22] measured the volumetric mass transfer coefficients, k_La, for the absorption of bubbled and unbubbled CO_2 in presence of surfactants. The results of experiments showed a dependency of k_La on stirring rate, type of bubbling device and surfactant concentration in the liquid phase. In other work [23], they considered the impact of surfactant in the bubble columns, and showed that the presence of the surfactant induces reduction of the interfacial area as well as the individual transfer coefficient of bubbles.

For Reynolds numbers below 100, Takemura and Yabe [24] investigated the bubble rise velocity and dissolution rate of carbon dioxide bubbles in slightly contaminated water. They compared the experimental results with numerical results developed by stagnant cap model and proposed equations for estimating the drag coefficient and Sherwood number and clarified that the gas–liquid interface of the carbon dioxide bubbles ranging 0.2 mm<d<1 mm in water are immobile. For bubble columns and air lift, Vasconcelos et al. [25] indicated that the values of liquid side mass transfer coefficient, k_L, always lie between the theoretical values for fully mobile and rigid interfaces. The results were analyzed based on the modelling of the kinetics of single bubble contamination and in accordance with the stagnant cap model. Calculated and experimental k_L values agreed within ±30%. Loubière and Hébrard [26] studied the effect of liquid surface tension on the bubble formation from both rigid and flexible orifice. The results showed that the effect of surface tension on the generated bubbles cannot be considered only in terms of the static surface tension and also depends on whether the bubbles are

produced from a rigid orifice or from a flexible orifice. Alves et al. [27] systematically investigated individual stationary air bubbles of 1–5 mm in a downward liquid flow. They interpreted both the drag coefficient and mass transfer coefficient based on the bubble contamination using the stagnant cap model and showed that the mass transfer coefficient for clean front and stagnant cap are consistent with theoretical prediction of Higbie´s and Frössling´s equations, respectively. In another study [28] they investigated the effect of Polyethylene glycol (PEG) on the average mass transfer coefficient, k_L, in an aerated stirred tank. The results indicated that bubbles in surfactant (PEG) solution behave as rigid bubbles, while bubbles in tap water behave closer to having a mobile interface and bubbles in salt solution have intermediate k_L values.

The buoyancy-driven motion of bubbles and drops in a vertical small tube was studied by Almatroushi and Borhan [29]. The results showed that the presence of a surfactant slows down the motion of small bubbles due to the development of adverse Marangoni stresses, while it increases the motion of large bubbles by allowing them to deform away from the tube wall more easily. Painmanakul et al. [30] investigated the effect of surfactant on bubble generation, interfacial area and the mass transfer rate in the dynamic bubble regime (Re=150-1000). It was clearly shown that the presence of surfactants affects the bubble generation and thus the interfacial area, and the liquid-side mass transfer coefficient, k_L, and proved that the surface coverage ratio is crucial for predicting the changes of k_L in aqueous solutions with surfactants. The effect of anionic, cationic and non-ionic surfactants on the mass transfer rate of bubbles in a small-scale bubble column was examined by Sardeing et al. [31]. They found three zones in the mass transfer coefficient as a function of bubble dimeter and showed that Higbie´s model does not predict the k_L values for large bubbles. Rosso et al. [32] prepared an experimental apparatus to concurrently measure dynamic surface tension and mass transfer for single and multi-bubbles. They showed that for a constant contamination, interfaces with higher renewal rates have higher dissolution rate and concluded that higher interfacial flow regimes can compensate contamination.

Effect of surface tension on pressure drop in a 1mm-square microchannel was investigated by English and Kandlikar [33],[34]. They applied water-surfactant mixtures of different concentrations and the accuracy of various two-phase pressure drop models was evaluated, and a new model for laminar-

laminar two-phase flow pressure drop was developed. Takagi et al. [35] investigated the dependence of the motions of a 1mm bubble rising through the laminar shear flow on 1-, 3-Pentanol and Triton X-100 concentration using a high-speed camera. The results confirmed that a bubble with larger Marangoni effect has smaller lateral migration. Furthermore, it was indicated that lower contaminant level and higher shear rate lead to a remarkable bubble migration toward the wall, which causes the development of bubble clusters. The effect of high concentration of surfactants on liquid side mass transfer coefficient in free gas–liquid interface was examined by Hebrard et al. [36]. A reduction in the mass transfer coefficient with an increase of surfactant concentrations was detected as well as a plateau when the concentration reaches critical micelle concentration (CMC); the smallest value was observed for a pure solution of surfactant. Jamnongwong et al. [37] examined the effect of presence of various substances commonly encountered in biological media on oxygen diffusion coefficient and liquid-side mass transfer coefficient. The results indicated that for all cases, oxygen diffusion coefficients decreased when compared to clean water, and, the rate of change of oxygen diffusion coefficient, D_c, is directly related to the type of substance. In bubbly channel flow, Takagi and Matsumoto [38] reviewed the recent investigations associated with subsequent variation of bubble behavior due to the surfactant adsorption/desorption on the bubble surface and concluded that the presence of surfactants influences the small-scale behavior of each bubble, and then this variation in bubble behavior causes a large-scale variation of global bubbly flow structures, which further influences each bubble's behavior.

The influence of surfactant addition and sparger design on the mass transfer, the gas holdup and bubble size distribution in a bubble column was compared by McClure et al. [39]. The results showed that addition of both hydrophilic and hydrophobic surfactants cause an approximately threefold decrease in mass transfer coefficient and presence of surfactant has a greater effect on oxygen dissolution than do changes in the sparger design. Huang and Saito [40] applied the laser-induced fluorescence (LIF/HPTS) method to investigate the effect of bubble-surface contamination on the relationship between instantaneous mass transfer, bubble motions, and bubble-induced surrounding liquid motions. They showed that in the contaminated water, because of desorption of surfactants and the Marangoni convection on the bubble surface, the mass transfer oscillates in accordance with

bubble velocity and the Marangoni convection altered both the liquid motions near the bubble surface and the bubble wake. Recently, Aoki et al. [41] investigated the effect of concentration of surfactant on the rate of mass transfer for single rising bubbles. They used Triton X-100 as surfactant and showed that for small bubbles the mass transfer rate reduces with increase of surfactant concentration and it however rises with the bubble size and approaches that of clean Taylor bubbles as for large bubble size. Furthermore, it was proved that the surfactant adsorbs only in the bubble tail region and the nose-to-side region is almost clean for large bubbles. In another work [42] they investigated the effect of type of surfactant on the mass transfer from single fully contaminated carbon dioxide bubbles. They showed that the k_L of contaminated Taylor bubbles have varying trends because of the difference in the surfactant distributions at the bubble interfaces which strongly depend on the Hatta number.

Table. 1 summarizes the main parameters of the known previous studies on the impact of presence of surfactant in gas-liquid two-phase interfaces, where d_{eq} is sphere-volume equivalent bubble diameter.

Table. 1. Previous studies on the impact of presence of surfactant in gas-liquid two-phase flows

Reference	Contact device	Gas / Liquid / Surfactant	Bubble/Channel dimensions	Parameter studied
Mancy and Okun [19]	Bubble column	O_2/water/Aerosol O.T.	$1.7 < d_{eq} < 2.4$ mm D = 220 mm	Mass transfer coefficient Bubble volume
Griffith [20]	Bubble column	Carbon-tetrachloride/glycerine/ Aerosol O.T., O.S.	D = 100 mm	Bubble terminal velocity
Raymond and Zieminski [21]	Bubble column	CO_2/water/Aliphatic alcohols	$0.13 < d_{eq} < 0.2$ mm	Mass transfer coefficient Drag coefficient
Vizquez et al. [22]	Stirred tank	CO_2/water/Sodium lauryl solphate	$0.04 < d_{eq} < 0.2$ mm D = 143 mm	Mass transfer coefficient
Vizquez et al. [23]	Bubble column	CO_2/water /Sodium lauryl solphate, sodium carbonate, sodium arsenite	$4.6 < d_{eq} < 8.5$ mm D = 113 mm	Mass transfer coefficient Interfacial area
Takemura and Yabe [24]	Square vessel	CO_2/water	$0.1 < d_{eq} < 0.5$ mm D=40 mm square	Mass transfer coefficient Drag coefficient
Vasconcelos et al. [25]	Bubble column, rectangular airlift	O_2, air/water/Antifoam Sigma 289	$3 < d_{eq} < 5$ mm D = 92 , 17 mm	Mass transfer coefficient
Loubière and Hébrard [26]	Square vessel	Air/water/butanol sodium lauryl sulphate, fatty alcohol C12/18, lauryl dimethyl benzyl ammonium bromine	$0.5 < d_{eq} < 5$ mm D = 400 mm square	Bubble dimeter, Dynamic surface tension, bubble frequency
Alves et al. [27]	Stirred tank	Air/Water/sodium sulphate, PEG	$0.8 < d_{eq} < 3$ mm D = 29.2 mm	Mass transfer coefficient local gas hold-up local bubble size
Alves et al. [28]	Vertical tube	Air/distilled water, millipore water	$0.5 < d_{eq} < 5$ mm D = 22, 31 mm	Mass transfer coefficient Drag coefficient Rise velocity
Almatroushi and Borhan [29]	Capillary tube	Air/water/UCON LB-165, glycerol, sodium dodecyl sulfate (SDS)	$4.0 < d_{eq} < 15$ mm D = 7.96 mm	Bubble terminal velocity
Painmanakul et al. [30]	Bubble column	Air/water/Sodium lauryl sulphate, Lauryl dimethyl benzyl ammonium bromine	$3 < d_{eq} < 9$ mm D = 50 mm	Mass transfer coefficient Rise velocity Interfacial area
Sardeing et al. [31]	Bubble column	Air/water/Sodium lauryl sulfate, Lauryl dimethyl benzyl ammonium bromine, Fatty alcohol C12/18	$1 < d_{eq} < 8$ mm D = 50 mm	Mass transfer coefficient Rise velocity Interfacial area
Rosso et al. [32]	Square graduated column	Air/water/SDS, IAA	$d_{eq} < 5$ mm	Mass transfer coefficient Dynamic surface tension
English and Kandlikar [33],[34]	Square minichannels	Air/water/Triton DF-12	D = 1 mm square	Pressure drop
Takagi et al. [35], [38]	Bubble column	Air/water/1-, 3-Pentanol, Triton X-100	$d_{eq} = 1$ mm D = 7.27 mm	Rise velocity Drag coefficient
Hebrard et al. [36]	Agitated vessel	Air/water/Texapon	$d_{eq} > 1$ mm D = 65 mm	Mass transfer coefficient Diffusion coefficient
Jamnongwong et al. [37]	Agitated vessel	Air/water/NaCl, glucose, sodium lauryl sulphate	$1 < d_{eq} < 5.3$ mm D = 65 mm	Mass transfer coefficient Diffusion coefficient
McClure et al. [39]	Bubble column	Air/water/Sodium sulfite, 2-propanol, mannitol, Antifoam	$2 < d_{eq} < 40$ mm D = 190 mm	Mass transfer coefficient Interfacial area
Huang and Saito [40]	Square channel	CO_2/water/1-pentanol	$d_{eq} = 2.9$ mm D = 15 mm square	Bubble shape and motion
Aoki et al. [41], [42]	Vertical tube	CO_2/water/Triton X-100, 1-octanol	$5 < d_{eq} < 30$ mm D =12.5, 18.2, 25.0 mm	Mass transfer coefficient Rise velocity Bubble shape

As mentioned above, most attention has been paid so far to the small spherical bubbles in infinite liquid regarding the effect of surfactant on the mass transfer rate. However, non-spherical large bubbles in small channels, which mainly exist in micro- and milli-channels in the form of Taylor bubbles, were the subject of only a few studies [42],[31]. On the other hand, regarding the influence of surfactant on the liquid film thickness for elongated bubbles in capillaries almost all of the investigations are theoretical and according to our knowledge very few experimental evidences could be found [16]. In addition, among the available theoretical investigations, in some references it was shown that surfactant has a thickening effect on the liquid film thickness whereas in others a thinning influence was found [12],[16],[43].

In the present work, the effect of surfactant on the shape, dissolution rate and liquid film thickness of an individual elongated Taylor bubble of CO_2 into the water, whose motion is governed by the tube walls, was investigated in channels of 6 mm inner diameter using a microfocus X-ray radiography technique. The bubbles were held stationary using the technique of Schulze and Schlünder [44] and the overall liquid side mass transfer coefficient was determined from microfocus X-ray images with high accuracy. The X-ray method was chosen since it is not dependent on refractive index. Therefore, it can be the most accurate in comparison with other conventional optical methods.

2 Materials and methods

To investigate the interaction between a single bubble and the liquid flowing around the bubble the dynamics of the shape of bubbles were radioscopically monitored. The acquired X-ray images of the bubbles were analyzed with respect to volume, surface area and length of the bubble.

2.1 Experimental

2.1.1 Setup

The apparatus, procedure and measurement calibration used in this study have been described in detail elsewhere [45],[46]. Thus only a brief description will be given here. The experimental setup is schematically shown in Fig. 1. A glass channel with circular cross section (300 mm length, 5.96 mm hydraulic diameter, made of borosilicate glass, wall thickness of about 2 mm) is placed between a microfocus X-ray source and a two-dimensional flat panel X-ray image detector. The capillary is

mounted between X-ray source and a two-dimensional flat panel X-ray image detector at the hollow shaft of a rotary table. Counter-current liquid flow through the capillary originating from the upper reservoir to the lower reservoir enables the fixation of the bubble at a given axial position in the capillary. Therefore, the flow rate had to be precisely adjusted and was remotely controlled by a motorized needle valve and was measured by calculating the accumulation of the drained liquid inside a graduated cylinder by a high-resolution camera as a function of time. A Taylor bubble is generated by the injection of some finite amount of gas into the liquid through a metallic needle aligned in parallel with the capillary. The amount of gas injected into the liquid is controlled by a remotely operated fast acting solenoid valve. Gas is provided either from a gas cylinder (laboratory CO_2 bottle, 99.99% purity) or a pressurized air supply. For reference measurements, the solenoid valve was replaced by a syringe and a defined volume of gas was inserted into the liquid. The water used for preparation of aqueous solutions, comes from an ion exchanger and was purified via a Millipore water purification system with output water having TOC (total organic carbon) 4 ppb and pH 7.0, was fed into the open-air overhead reservoir. The reservoir was covered by a plastic head to prevent intrusion of dust particles; however air would dissolve in the water during the experiments. The temperature was fixed at about 294±1 K. A level indicator was installed in the upper reservoir to indicate the hydraulic static pressure.

The nonionic compound Triton X-100 ($C_8H_{17}C_6H_4(OCH_2CH_2)_{10}OH$) was used as surface active agent to contaminate the millipore water. It is a commonly used detergent in laboratories or cleaning materials. Surfactant concentrations C_s were set to 0.4, 2.0 and 20.0 mmol/m^3 (0.26, 1.30 and 13.0 ppm, respectively), which are much lower than the critical micelle concentration (240 mmol/m^3) [10] and the change of the viscosity can be negligible. The concentration of surfactant was selected based on the most common ranges used by other investigators in the literature [42],[41],[38],[35],[10] for gas liquid systems and to compare the effect of concentration, lower and higher concentrations were applied. In our experimental set up, the maximum surfactant concentration which could be applied was about 13.0 ppm (20 mmol/m^3). However, due to type of gas injection system, applying higher concentration of Triton X-100 caused foaming which considerably reduced the accuracy of

measurements. The physicochemical properties of surfactant [10] based on the Langmuir isotherm [41] to calculate the surface coverage ratio, *Se*, are as follows:

$$La = \frac{C_s \beta}{\alpha} \quad (1)$$

$$S_e = \frac{La}{La+1} \quad (2)$$

The surface coverage ratio is defined as the ratio of interfacial surfactant concentration at equilibrium to the saturated interfacial surfactant concentration and *La* is dimensionless Laplace number. α and β are desorption and adsorption rate constant and their values are 0.033 s^{-1} and 50 $m^3mol^{-1}s^{-1}$, respectively [10]. *Se*, *La*, and surface tension, σ, measured for liquid phase are shown in Table. 2.

Table. 2. Physicochemical properties of liquid phase

	0.26 ppm Triton X-100	1.3 ppm Triton X-100	13.0 ppm Triton X-100
Surface tension [N/m]	0.0677	0.0620	0.0510
Laplace number	0.61	3.03	30.30
Surface coverage ratio	0.38	0.75	0.97

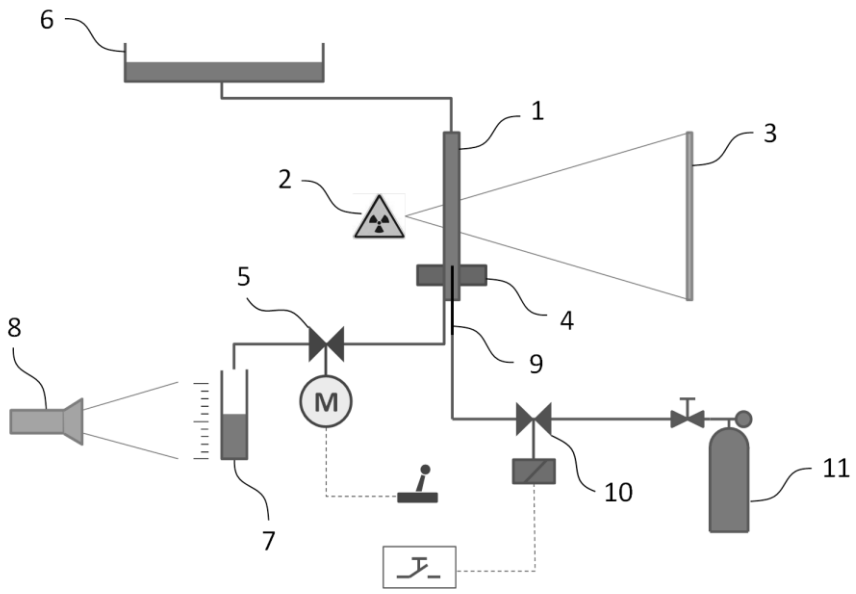

Fig. 1. Schematic drawing of the experimental setup: 1 – observation section, 2 – microfocus X-ray source, 3 – flat panel X-ray image detector, 4 – rotary table, 5 – remotely controlled motorized needle valve, 6 – upper reservoir, 7 – lower reservoir, 8 – video camera, 9 – injection needle, 10 – fast solenoid valve, 11 – gas cylinder

2.1.2 Procedure

Before the onset of the experiments a high countercurrent flow rate was applied and a large number of bubbles was injected into the liquid to flush the injection needle and pipes and to ensure that they were

filled with the injection gas only. At the beginning of the experiments a number of reference images were acquired for the liquid filled capillary. The low flow rate was applied at the beginning of the experiment. Then, a bubble was injected into the liquid. As soon as the ascending bubble reached the field of view, the motorized valve was actuated to increase the liquid flow and to keep the bubble stationary. A sequence of X-ray images was acquired while the bubble dissolved into the liquid. As the volume of the bubble shrank, the velocity of the bubble changed. Thus, the flow rate had to be continuously adjusted.

2.2 X-ray image acquisition

2.2.1 X-ray source

A microfocus X-ray tube (X-RAY WorX XWT-190-TC) equipped with a tungsten high energy transmission target was used as radiation source. Maximum tube voltage was 150 kV at a maximum target power of 25 W. However, a tube voltage of 135 kV and a tube current of 40 µA were used in order to not exceed 5W target power and to achieve the smallest focal spot size and thus highest spatial resolution. The X-ray parameters were held fixed during all experiments.

2.2.2 X-ray detector

A two-dimensional flat panel X-ray detector (Perkin Elmer XRD 0822 AP3 IND) equipped with a high efficiency/high resolution cesium iodine (CsI) scintillation screen was used as image detector. The resolution of the detector is 1024 x 1024 px at a pixel size of 200 µm x 200 µm. Thus the detector covers an area of 200 mm x 200 mm. An integration time of 100 ms per image was chosen for the radioscopic measurements. The shrinking Taylor bubble was radioscopically monitored with an exposure time of 100 ms and a frame rate of 5 Hz.

2.3 X-ray image processing

From the acquired radioscopic data extinction images E were calculated according to

$$E_{ij} = \mu d_{ij} = -log\left(\frac{I_{ij}}{I_0}\right) \qquad (3)$$

where μd describing the extinction (linear extinction coefficient times X-ray path length) along each individual ray path between source and detector pixel ij. The reference intensity measured at the detector without any object in the X-ray beam is given by I_0, while I is the measured intensity with the capillary in view. The cylindricity of the circular glass channel was checked using the microfocus X-ray computed tomography and the diameter was found to vary by 0.5%, and the inner diameter of the channel was determined to be 5.96 ± 0.03 mm. With the known inner tube diameter all X-ray images were geometrically calibrated to an effective pixel spacing of 27.4 µm ± 0.5%.

In order to quantify the bubble's length, volume and interfacial area, an extinction image E_b showing the Taylor bubble only was computed by subtraction

$$E_b = E_g - E_{ref}, \qquad (4)$$

as exemplarily given in Fig. 2a. The bubbles interface was extracted from these extinction images by detection of the edges of the projected bubbles. A resulting fully reconstructed two-dimensional projected bubble interface is shown in Fig. 2b.

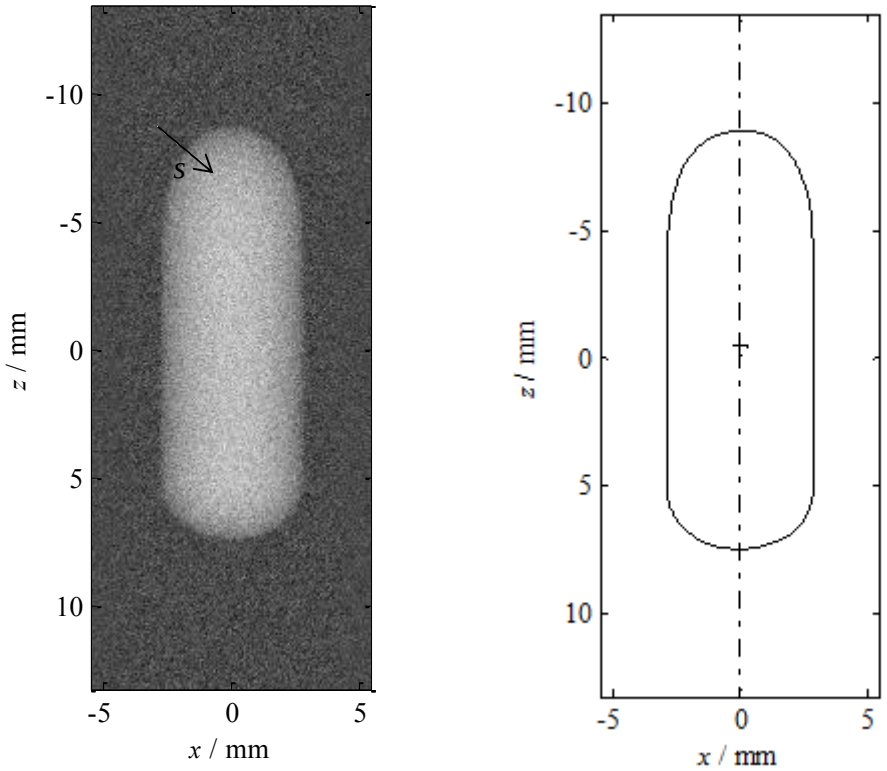

Fig. 2. (a). Extinction image of a Taylor bubble (raw data), the arrow indicates a scanline normal to the projected interface, (b). Extracted bubble interface projection (solid line)

The bubble's length L_b is computed by the difference of the maximum and minimum z-position of the extracted projected bubble interface.

For the circular channel, the fully three-dimensional bubble shape could be retrieved by rotational expansion of the two-dimensional interfacial curve by revolution around its axis. However, it turned out that the fixation of the vertical position of the bubble by remote controlling of the flow rate turned out to be rather difficult and slight motion of the bubble occurred during the experiments. Due to the finite exposure times of the X-ray detector the bubble motion causes blurring of the front and rear interface in the bubble projection. This causes the bubbles to appear at different sizes than they actually are. Therefore, eventually only the integral extinction $\sum_{ij} E_{ij}$ was considered when analyzing the bubble's dissolution rate, and the bubble's volume and interfacial area are computed via calibration function k_V and k_S,

$$V_b' = k_V \sum_{ij} E_{ij} \quad (5)$$

$$S_b' = k_S \sum_{ij} E_{ij} \quad (6)$$

2.3.1 Calibration

The bubble volume and interfacial area were computed for each image E_b utilizing calibration functions k_V and k_S (Eq. 5 and 6). The latter were derived from dedicated calibration experiments as follows. Non-dissolving air bubbles of different size were injected into the liquid filled capillary and were held at a fixed position by application of a countercurrent flow. Since the bubbles were not shrinking, disturbing bubble motion was not present during the calibration measurement. An average extinction image $\overline{E_b}$ of the non-dissolving bubble was generated by integration of 256 single images, which increased the signal to noise ratio by a factor of 16. To extract the projected bubble interface the image $\overline{E_b}$ was scanned along lines normal to an anticipated interfacial curve. An ellipse was fitted to the scanned extinction signal to eventually detect the edge of the projected bubble at the interception of the ellipse with the base line. Construction of a solid of revolution from the extracted two-dimensional projected interfacial curve enabled precise measurement of the volume and interfacial area of the reference bubbles. The relative error in the measurement of the projected interfacial curve is estimated to be ±1 px, thus resulting in an uncertainty in the volume and interfacial area measurement of $\delta V_b/V_b = 3.8\%$ and $\delta S_b/S_b = 2.3\%$ including the uncertainty of the pixel spacing. Relating the measurements to the integral extinction $\sum_{ij} E_{ij}$ by a linear regression resulted in the factors k_V and k_S.

2.4 Mass transfer coefficient calculation

For a CO_2 bubble absorbing into water, the resistance to mass transfer in the gas phase is negligible with respect to the resistance in the liquid phase under the prevailing conditions [6]. Therefore the rate of mass transfer is proportional to the difference of interface and bulk concentration of liquid phase

$$-\frac{dn}{dt} = k_L A(C^* - C). \quad (7)$$

In this equation n is the total moles of gas phase (CO_2) inside the bubble, t the time, C^* the concentration of gas at the interface and C concentration of gas in the liquid bulk. Assuming the equilibrium at the interface by the Henry's law and since $C<<C^*$, we have

$$\frac{dn}{dt} = -k_L A \frac{C_L P y}{H - P y}, \quad (8)$$

where H is the Henry's constant, C_L the water concentration, y the mole fraction of CO_2 inside the gas phase and P the pressure inside the bubble calculated by

$$P = P_{atm} + \rho_L g h . \quad (9)$$

Here P_{atm} is atmospheric pressure, h the distance from the liquid surface in the upper reservoir and center of the bubble, which is constant for all experiments. Due to atmospheric pressure of the bubble we can assume that the gas phase follows the ideal gas law, therefore we can replace dn/dt in terms of V_b (volume of bubble) as:

$$\frac{\mathrm{d}n}{\mathrm{d}t} = \frac{P}{RT}\frac{dV_b}{dt}, \quad (10)$$

where R is universal gas constant and T gas temperature.

Hosoda et al. [47] have shown that for the first several ten seconds from the injection of the bubbles the CO_2 composition inside the bubbles can be considered as unity. However, in our experiments to calculate the k_L, we only considered initial first seconds of CO_2 dissolution and as a result the counter diffusion from liquid to bubble is negligible. Therefore by assuming y as unity and by combining Eq. 9 and 10 we have

$$k_L = -\frac{1}{ART}\frac{H-P}{C_L}\frac{dV_b}{dt} . \quad (11)$$

The mass transfer was calculated by applying a difference scheme to determine dV_b/dt.

3 Results and discussion

3.1 Bubble shape and rise velocity

The free rise velocity of bubbles in the channel was precisely measured utilizing X-ray radiographic images. The position of bubbles in a height-range of 30 mm was traced and rise velocity was calculated. The measured data both for clean and contaminated bubbles are shown in Fig. 3. For comparison and evaluation of the measured data, a CCD video camera (AVT Pike F-100B) was used

for clean bubbles to measure the rise velocity. The bubble's position over a height-range of 100 mm at moderately high frame rates of 231.8 frames per second and at effective pixel resolution of 104 µm was continuously monitored. The difference between the measured bubble velocities for the two methods is less than 2%.

The prediction of the correlation proposed by White and Beardmore [48] is also presented in this figure. This correlation is proposed only for cylindrical bubbles in circular pipes, therefore it is not applicable for bubble lengths in the range of the channel diameter while the bubbles are not cylindrical. As it can be seen, for clean bubbles there is a good agreement between our experimental data and this correlation.

In addition, Fig. 3 shows that the rise velocity of small bubbles strongly depends on the bubble size and increases with decrease of bubble length (for clean bubbles when L_b<7.4 mm), while it remains constant for large bubbles (for clean bubbles when L_b>12 mm) and there is a transition region in between. In this region despite the shape of bubbles is still bullet shape and the bubble are elongated, there is a special bubble size (L_b = 9.8 mm) at which, bubble velocity reaches maximum value. This can be attributed to the interaction effect of viscous and interfacial stress on one hand and inertial and gravitational stresses on the other hand.

Furthermore, as it is shown, contamination affects the rise velocity of bubbles. For small bubbles, presence of surfactant causes to decrease the rise velocity of bubbles while for elongated bubbles, contamination causes the increase of bubble velocity. These findings are in accordance with the other theoretical and experimental findings [8],[10],[49]. Almatroushi and Borhan [29] reported the same findings for bubbles contaminated by sodium dodecyl sulfate (SDS) in a circular pipe of 7.9 mm hydraulic diameter and showed that the surfactant decreases the motion of small bubbles because of development of adverse Maragoni stresses, while it enhances the mobility of large bubbles by increasing their deformability away from the tube wall.

Besides, as it can be seen, for clean and high contaminated solution (13.0 ppm Triron X-100), the values of rise velocity of bubbles both for small and elongated bubbles show stable trend, while for low and intermediate concentration of surfactant (0.26 and 1.30 ppm), the data points for elongated bubbles are somehow scattered and for small bubbles no scattering could be observed. The reason

could be attributed to the influence of surfactant concentration on the shape of long bubbles. Hayashi and Tomiyama [10] have shown that the rise velocity of elongated Taylor bubbles is related to the nose curvature of the bubbles which is mainly governed by interfacial tension. Fig. 4a shows the extracted interface of a single Taylor bubble in clean and contaminated solutions of Triton X-100. As it can be seen, the bubble nose in higher concentration of surfactant has the maximum curvature in comparison with bubbles in clean and lower contaminated systems (Fig. 4b). The bubble nose curvature in low contaminated systems is almost the same as of clean bubble. However, as it can be detected in Fig. 4c, the bubble shape and curvature in lower contaminated systems start to deviate from clean bubble shape and approach to the high contaminated system in the middle of the bubble length. This change and transition in shape of bubble from clean to high contaminated could be a possible reason that the values of rise velocity of bubbles in low contaminated systems scatter between the rise velocity values in clean and high contaminated systems.

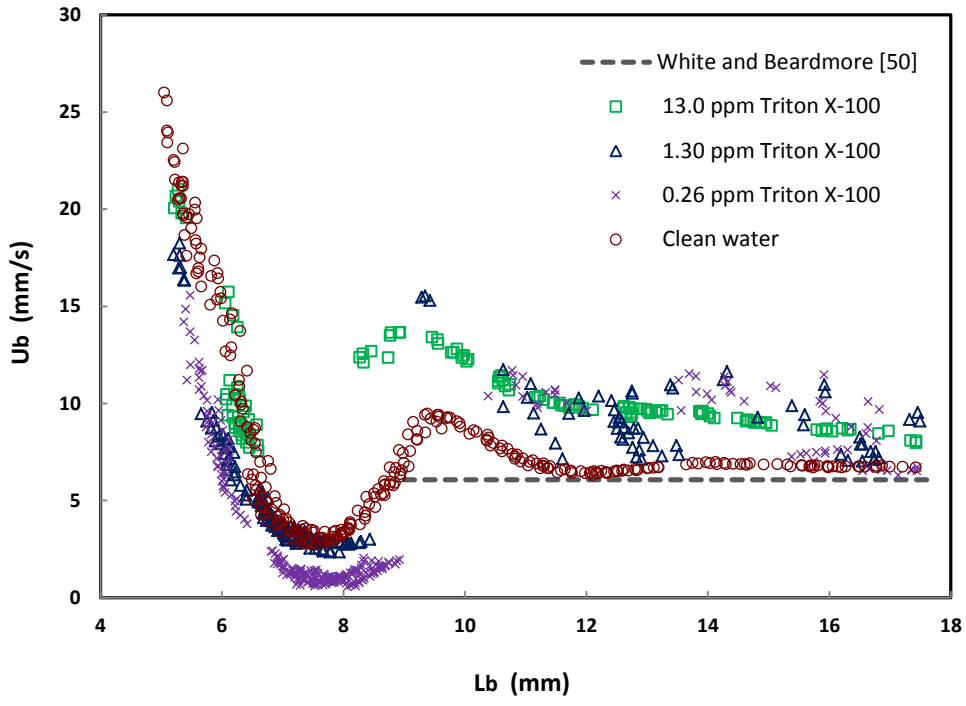

Fig. 3. Bubble rise velocity as a function of bubble length in clean and contaminated water

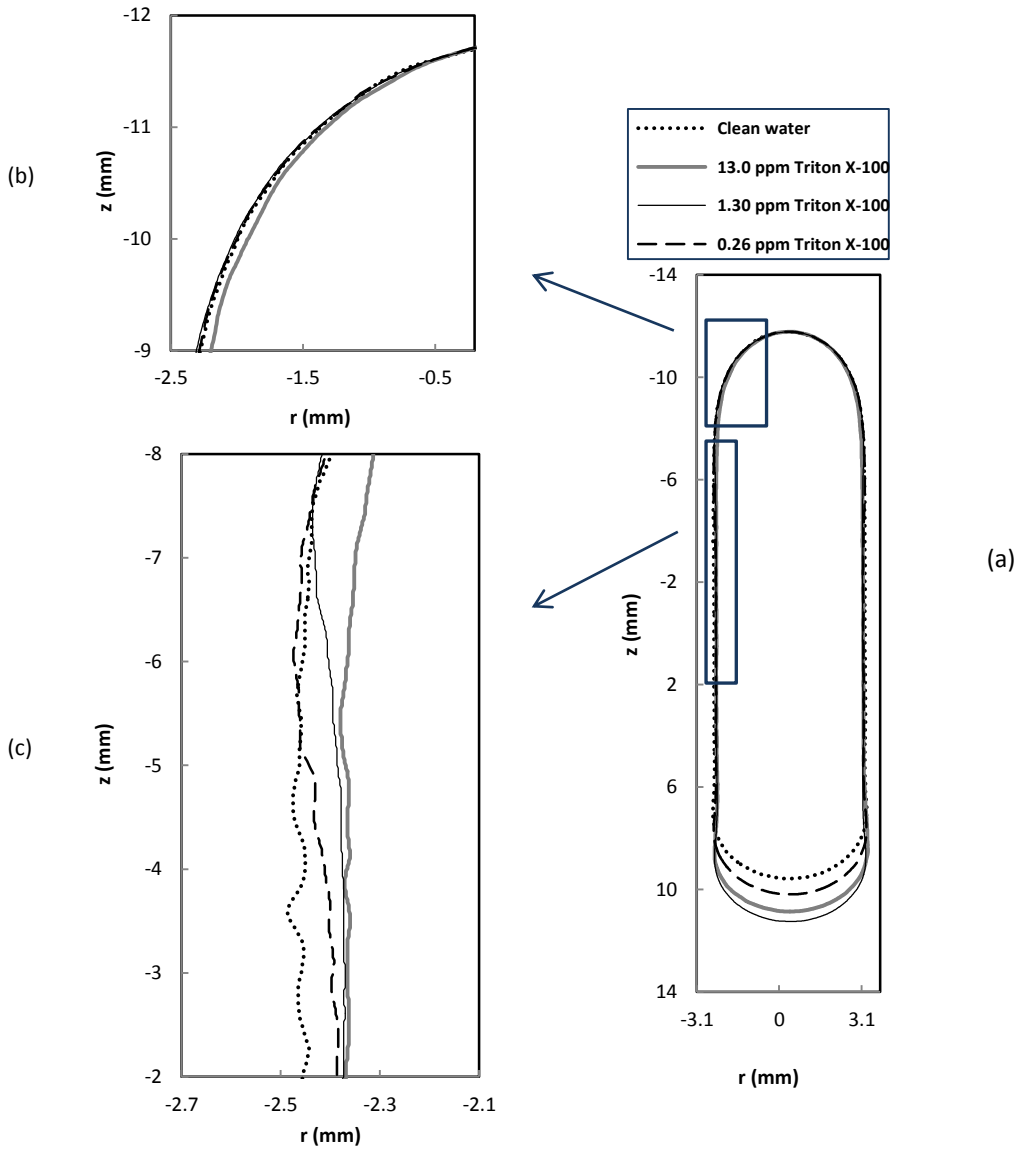

Fig. 4. Extracted bubble interfaces, comparison between bubble curvature in clean and contaminated water

An example of instantaneous X-ray radiographic bubble images in 5.96 mm diameter channel in clean and contaminated water are shown in Fig. 5. The nose and tail of the large Taylor bubbles both for clean and contaminated system are stable and no oscillations were observed in their shape. For smaller bubbles there exist some small shape oscillations, however, for bubbles in clean water with equivalent diameter below channel diameter, strong zig-zag movement and shape oscillations were observed (Fig. 5a,b) while no bubble movement and shape oscillation were detected for contaminated bubbles (Fig. 5g,h).

Furthermore, the impact of bubble shape and dimensions on the rise velocity of bubbles can be detected in Fig. 5. In this figure V_b is bubble volume, L_b bubble length and d_{max} bubble diameter at its maximum cross section in the channel. d_{max} which indirectly shows the minimum available gap between the bubble and the channel wall for liquid flow, remains almost constant for large elongated bubble (for example Fig. 5e and f), correspondingly, it was shown in Fig. 3 that bubble rise velocity does not change for large bubbles.

On the other hand, at bubble length about 10 mm, d_{max} reaches the minimum value among the elongated bubbles, while the bubble rise velocity is maximum around this bubble size as is shown in Fig. 3 and corresponds to the maximum bubble rise velocity in transition region. As a result, it can be concluded that the changes in the rise velocity of bubbles are in accordance with size and also the shape of the bubbles in small channels.

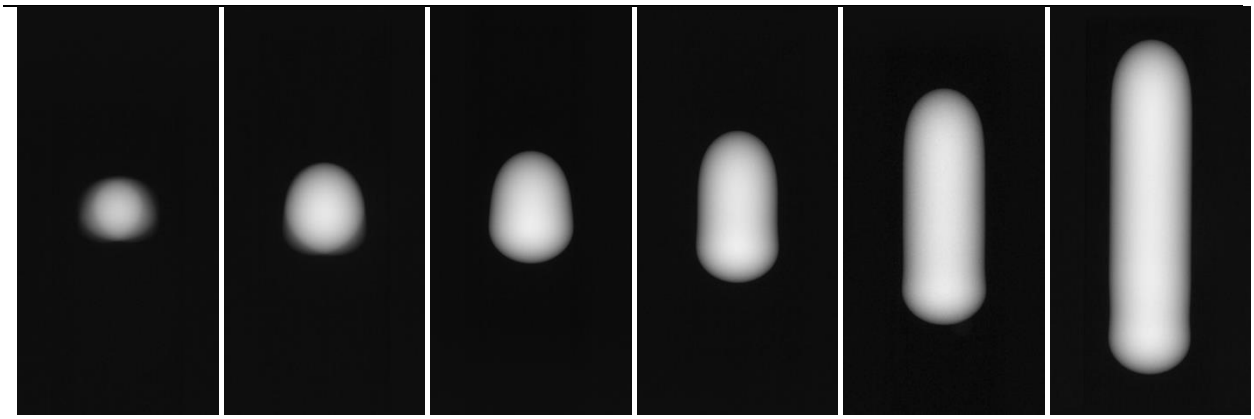

(a)	(b)	(c)	(d)	(e)	(f)
V_b = 70.0 mm^3 L_b = 4.3 mm d_{max} = -	V_b = 112.3 mm^3 L_b = 6.4 mm d_{max} = -	V_b = 145.5 mm^3 L_b = 7.8 mm d_{max} = 5.84 mm	V_b = 207.2 mm^3 L_b = 10.5 mm d_{max} = 5.73 mm	V_b = 357.3 mm^3 L_b = 16.2 mm d_{max} = 5.81 mm	V_b = 523.5 mm^3 L_b = 23.4 mm d_{max} = 5.81 mm

Clean water

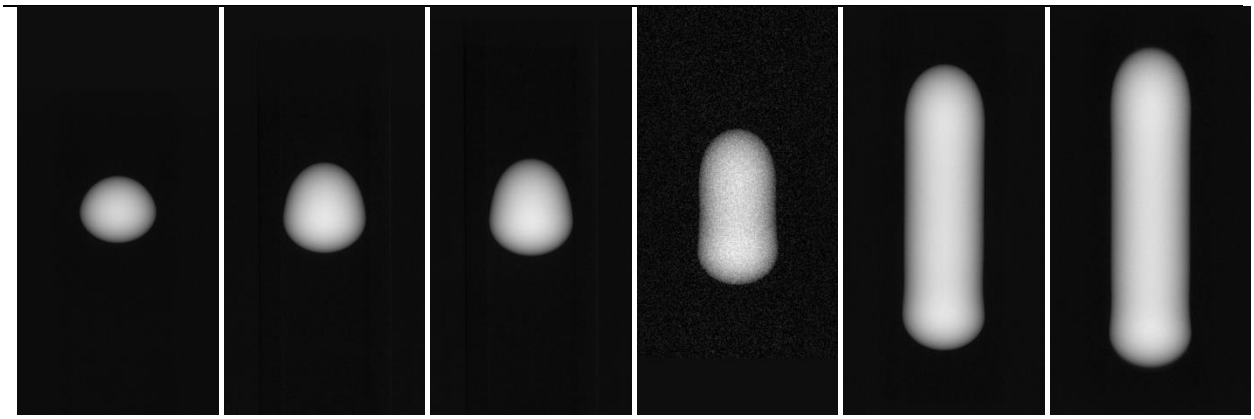

(g)	(h)	(i)	(j)	(k)	(l)
V_b = 66.1 mm^3 L_b = 4.6 mm d_{max} = 5.28 mm	V_b = 106.8 mm^3 L_b = 6.2 mm d_{max} = 5.71 mm	V_b = 117.3 mm^3 L_b = 6.7 mm d_{max} = 5.75 mm	V_b = 202.2 mm^3 L_b = 10.2 mm d_{max} = 5.64 mm	V_b = 422.9 mm^3 L_b = 18.8 mm d_{max} = 5.69 mm	V_b = 476.8 mm^3 L_b = 21.9 mm d_{max} = 5.69 mm

Contaminated water (Triton X-100 1.3 ppm)

Fig. 5. Bubble radioscopic images as a function of bubble size

3.2 Bubble shape and liquid film thickness

Fig. 6 shows few examples of extracted bubble interface profiles with various sizes in clean and contaminated water. As it can be seen, the presence of surfactant causes a slight increase of the liquid film thickness around the bubble and as a result the elongation of contaminated bubble.

In our case where the concentration of surfactant in the liquid bulk is low (far away from CMC), the surfactants are absorbed onto the bubble interface and convected towards the stagnation point on the end of the bubble where they are accumulated. This interfacial shear generated by the flowing contaminated liquid around the bubble causes the development of a surface traction in the direction of

the film (Marangoni stresses) which leads to push more fluid into the thin liquid film region and consequently causes an increase in liquid film thickness and elongation of the bubble [13],[18].

This problem was firstly raised by Bretherton [50]. He theoretically analyzed displacement of long bubbles in a capillary and showed that the wetting film thickness left behind the bubbles is proportional to $Ca^{2/3}$. In the range of $Ca < 10^{-4}$, however, his model under predicts the liquid film thickness. Bretherton [50] proposed that adsorbed impurities on the surface of bubbles may cause the discrepancy between the theory and experiment. Several investigations confirms the thickening effect of impurities both analytically [13],[14],[15],[51] and numerically [10],[52],[18] and proved that the observed discrepancy of the liquid film thickness at low *Ca* is due to the dominant role of Marangoni effects in that limit . However, almost all of experimental studies have been done in this subject, focused mainly on the fiber coating known as Landau-Levich problem [18] and the present work might be one of the first experimental evidence of film thickening of finite-size bubbles in small channels.

The measured liquid film thickness around the bubble at the center of mass of the bubbles for a large range of bubble lengths is shown in Fig. 7. The film thickness values listed in this figure are averages of at least five measurements. The error bars indicating one standard deviation about the mean are in (or smaller than) the size of the data points.

In Fig. 7 the effect of surfactant concentration on the film thickness of elongated bubbles, are examined by applying three different concentration of Triton X-100. As it is shown, increase of contamination causes a slight increase in liquid film thickness and its trend is consistent with the results of previous experimental and analytical investigations [18],[53]. For example, Olgac and Muradoglu [18] showed that the thickening effect of surfactants grows up as the surfactant concentration increases.

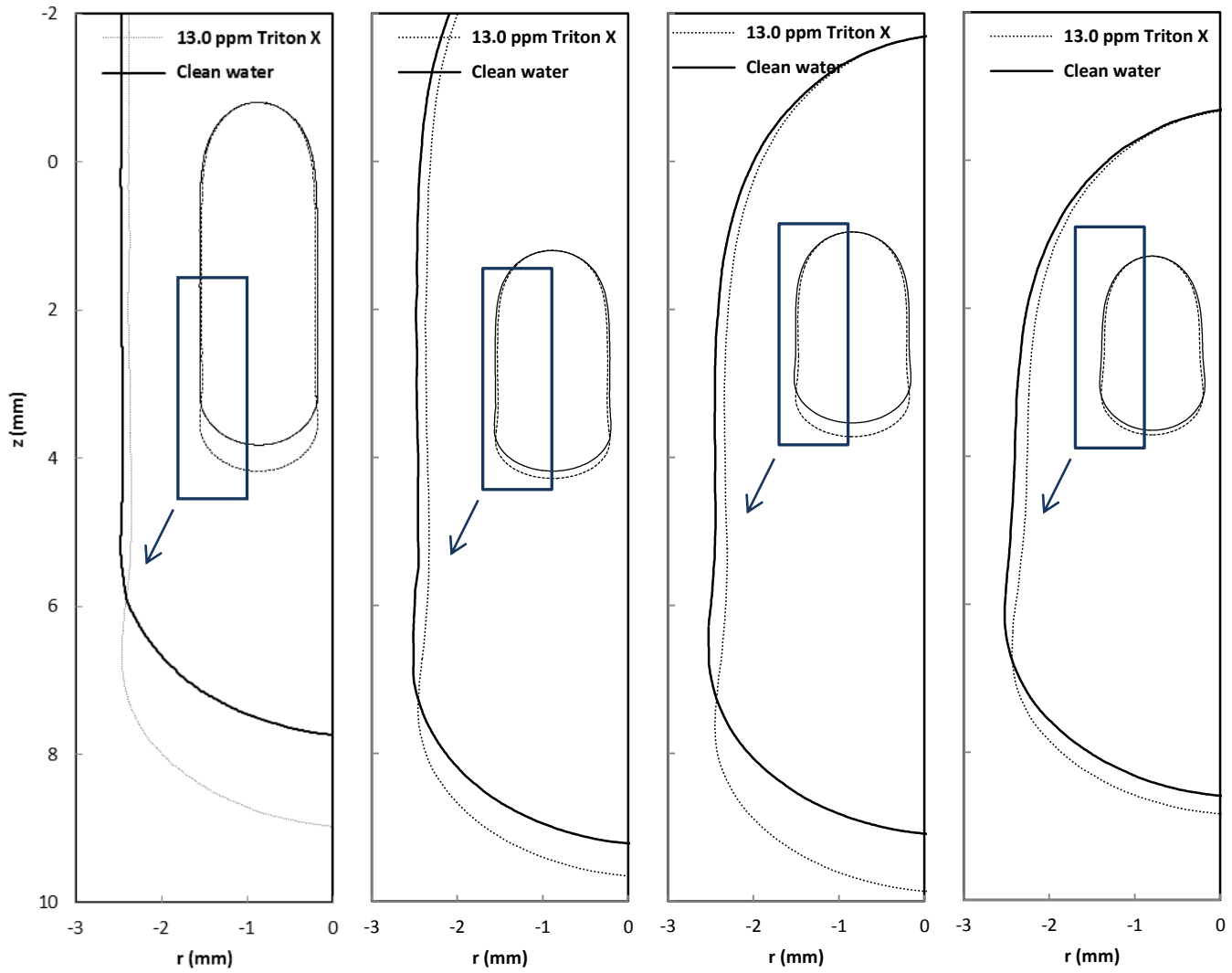

(a)		(b)		(c)		(d)	
Clean bubble	**Contaminated**	**Clean bubble**	**Contaminated**	**Clean bubble**	**Contaminated**	**Clean bubble**	**Contaminated**
V_b = 358.2 mm^3	V_b = 364.6 mm^3	V_b = 282.8 mm^3	V_b = 272.0 mm^3	V_b = 222.0 mm^3	V_b = 222.7 mm^3	V_b = 179.8 mm^3	V_b = 171.7 mm^3
L_b = 16.26 mm	L_b = 17.44 mm	L_b = 13.23 mm	L_b = 13.63 mm	L_b = 10.86 mm	L_b = 11.59 mm	L_b = 9.33 mm	L_b = 9.55 mm

Fig. 6. Extracted bubble interfaces, comparison between clean and contaminated water

However, the film thickening effect of surfactant with increase of contamination is not high. The reason can arise from the fact that the range of change of surfactant concentration used in our study does not have a significant effect on the interfacial surface tension of phases. In our case, increase of surfactant concentration from 0.26 ppm to 1.30 ppm causes a reduction of only 8% in the surface tension and rise of Triton X-100 concentration from 1.30 ppm to 13.0 ppm leads to decrease of 17% in the interfacial tension.

The measured interface of clean and contaminated bubbles are presented in the form of polynomials and summarized in Appendix A.1.

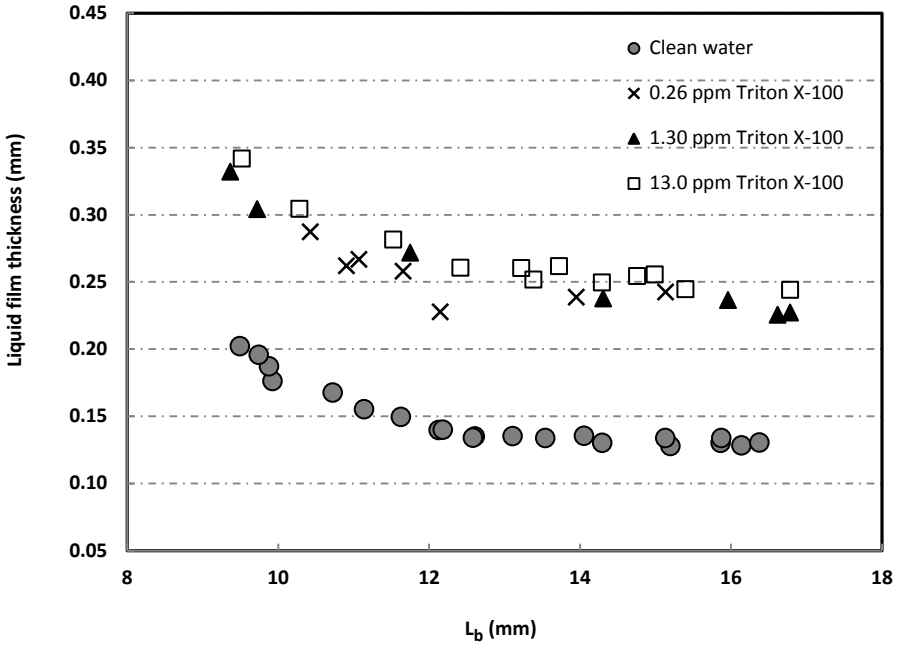

Fig. 7. The measured liquid film thickness around the bubble at the center of mass of the bubbles

3.3 Mass transfer coefficient

The liquid side mass transfer coefficients, k_L, according to Eq. (20) for single bubbles in pure and contaminated water are presented in Fig. 8. The values of mass transfer coefficients plotted in this figure are averages of at least five measurements. The error bars indicate one standard deviation about the mean points.

As it can be seen, contamination causes a reduction of the mass transfer coefficient for both small and elongated bubbles. The retardation of the mass transfer coefficient in presence of surfactant concentration can be attributed to either the hydrodynamic influence or to the formation of an interfacial barrier layer [54]. The influence of surfactant on the hydrodynamics of a moving bubble may cause modifications in the internal circulation velocities, reducing interfacial waves, and the hindrance of interfacial movement via the gradient of interfacial tension along the bubble surface (Marangoni effect) [55]. On the other hand, in the barrier layer model which also known as the physicochemical effect, the molecules of surfactant adsorb on the bubble interface and form a

condensed monolayer. As a result, the interfacial free area for the mass transfer is reduced. When the transferring spices transfers through the adsorbed layer on the interface, the interaction between the molecules of solute and surfactant becomes an additional resistance and the rate of mass transfer is decreased. Based on this model, the mass-transfer resistance will grow up with the rise in surface concentration of surfactant [54].

Furthermore, as it can be seen in Fig. 8, for the surfactant free system mass transfer coefficient decreases as the equivalent bubble size ratio increases, while in contaminated water k_L does not show any considerable dependency on the bubble size ratio. In other words, the comparison between clean and contaminated bubbles indicates that presence of surfactant has a more significant impact on the dissolution rate of small bubbles. The same trend was reported for ellipsoidal and Taylor bubbles in 12.5, 18.2 and 25.0 mm pipes in presence of Triton X-100 and 1-octanol solutions by Aoki et al. [41],[42]. They showed that the interface immobilization caused by the Marangoni effects is the reason for the decrease of k_L in small bubbles. For Taylor bubbles they found that mass transfer coefficients of contaminated bubbles are also smaller than those of clean bubbles, whereas they grow with bubble size and approach those of clean bubbles. The reason could be attributed to the interface mobility of bubbles while the mass transfer coefficient of dissolving bubbles is proved to depend upon interface mobility [56]. For clean water, the high mass transfer rate is related to the internal circulation of bubble, and the interfacial turbulence occurred with the mass transfer across an interface. For the contaminated system, the interfacial mobility will be inhibited by the Marangoni stress. Furthermore, it has been shown that contamination influences more considerably smaller bubbles [7], while concentration and surface tension gradients are more noticeable for ‘‘small’’ than for ‘‘large’’ bubbles, since their surface is less influenced by impurities and moves more freely [57]. This result is consistent with the findings concerning the rise velocity of small and elongated bubbles, while the rise velocity, shape oscillation and capillary waves of contaminated small bubbles are lower than for clean bubbles.

Furthermore, in Fig. 8 the influence of surfactant concentration on the mass transfer coefficient of single bubbles is evaluated. As it can be seen, for elongated bubbles, increase of surfactant concentration causes to decrease of mass transfer coefficient. For low concentration of surfactant (0.26

ppm), contamination causes a reduction of k_L by 29%. However, for higher Triton X-100 concentration (1.30 ppm and 13.0 ppm), mass transfer coefficient reduces to 55%. This is attributed on one hand to the physicochemical nature of used surfactant. The adsorption behavior of Triton X-100 was shown to follow the diffusion-controlled mechanism both at the air-water or the oil-water interfaces [58],[55]. As a result the rate of surfactant transfer can be grown up steadily by increasing the bulk concentration, which intensify the hydrodynamic influence of surfactant and causes further reduction in internal circulation velocities and interfacial mobilization and increase of Marangoni stresses along the bubble surface. On the other hand, the influence of surfactant concentration on k_L can be related to the surface coverage ratio of surfactant. Surface coverage ratio is directly affected by the concentration of surfactant or degree of contamination of the bubbles. In our case, for low surfactant concentration (0.26 ppm), *Se* is about 38% while this parameter is about 75% for 1.30 ppm solution and as it was mentioned before rise of surface coverage ratio strengthen the barrier layer effect of surfactants. As a result, increase of surfactant concentration which corresponds to the rise of the barrier resistance of surfactants may be another reason for decrease of mass transfer coefficient of elongated bubbles.

Furthermore, Fig. 8 shows that for higher surfactant concentrations (1.30 ppm), addition of concentration does not have any considerable influence on the k_L. In this case, increase of surfactant concentration from 1.30 ppm to 13.0 ppm which corresponds to change of *Se* from 75% to 97% indicates that at high surfactant concentration which corresponds to high coverage ratio, increase of contamination does not have a significant influence on the mass transfer coefficient of bubbles.

As it was mentioned, increase of surfactant concentrations to the CMC concentration was not possible due to the experimental limitations. However, for liquid droplets in aqueous phase, it is shown [54],[59],[60] that increase of surfactant concentration close to CMC can form a micelle zone at the trailing end of a bubble due to elevated surfactant concentration in the adjacent sublayer which causes partially remobilization of interface and consequently increase of mass transfer coefficient. Investigation of mentioned phenomena for gas bubble system would be the subject of future studies.

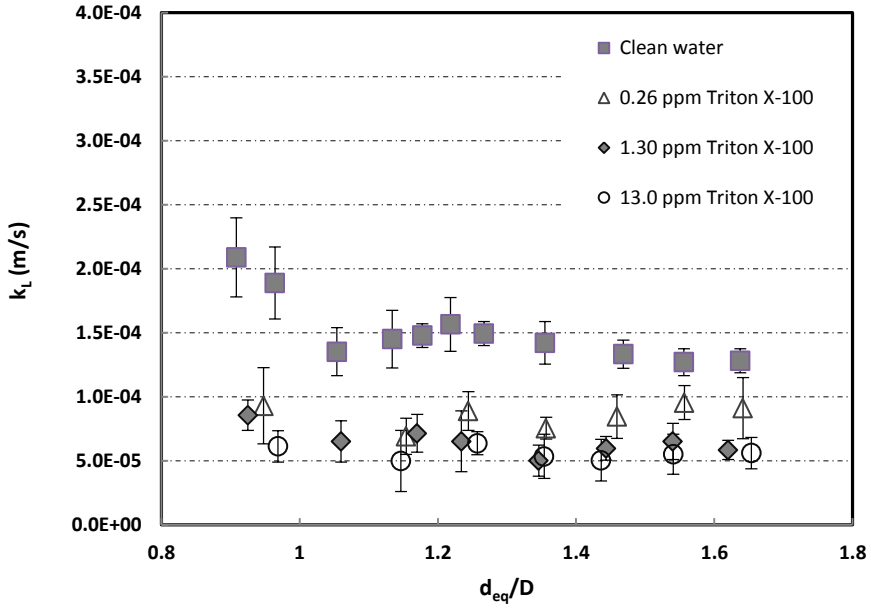

Fig. 8. Liquid side mass transfer coefficients for stagnant single bubbles in clean and contaminated water

4 Conclusions

The shape and absorption rate of an individual elongated Taylor bubble of CO_2 through contaminated water was measured in a millimeter-size channel to investigate the effect of surfactant. The bubbles were held stationary in the down-flowing liquid and the liquid side mass transfer coefficient was determined from microfocus X-ray images. The acquired X-ray images of the bubbles were analyzed with respect to volume, surface area and length of the bubble and were utilized to obtain the liquid side mass transfer coefficient and shape of the bubble. The comparison of the results for the clean and contaminated water showed that:

- A small amount of surfactant reduces the mass transfer of Taylor bubbles.
- Presence of surfactant has a more significant impact on the mass transfer rate of small bubbles.
- At high surfactant concentration which corresponds to high coverage ratio, increase of contamination does not have a noticeable influence on the mass transfer coefficient of bubbles.

- The presence of surfactants causes the change of the bubble shape and leads to a slight increase of the liquid film thickness around the bubble and as a result the elongation of contaminated bubble.
- The present work is an experimental evidence of film thickening effect of surfactants on the finite-size bubbles in small channels.

Acknowledgement

This work is funded by the German Research Foundation (DFG), priority program "Transport processes at fluidic interfaces", SPP 1506. The authors thankfully acknowledge the financial support.

Appendix A

A.1 Interface data of clean and contaminated bubbles

The interface data of clean and contaminated bubbles shown in Fig. 6 are fitted in the form of polynomials and presented in Table. A1. In this table, r_b is bubble radius, z is axial distance from the head of the bubble, a_0 to a_{20} are polynomial coefficients and dev_{max} is the maximum deviation in absolute distance between the interface sampling points extracted from the x-ray images and their nearest points on the fitted polynomial curve.

Table. A.1 Interface data of clean and contaminated bubbles shown in Fig. 6

$$r_b(mm) = a_{20}z^{20} + a_{19}z^{19} + a_{18}z^{18} + a_{17}z^{17} + a_{16}z^{16} + a_{15}z^{15} + a_{14}z^{14} + a_{13}z^{13} + a_{12}z^{12} + a_{11}z^{11} + a_{10}z^{10} + a_9z^9 + a_8z^8 + a_7z^7 + a_6z^6 + a_5z^5 + a_4z^4 + a_3z^3 + a_2z^2 + a_1z + a_0$$

Fig. 6	a		b	
Coefficients	**clean**	**contaminated**	**clean**	**contaminated**
a_{20}	-4.80294695935788E-15	-9.40421305721929E-16	-1.24211940306675E-14	-2.24049589508817E-14
a_{19}	7.79266701796566E-13	1.62440851637228E-13	2.36763272004498E-12	2.97693316128133E-12
a_{18}	-5.85750889133396E-11	-1.29930403099477E-11	-2.09173218752898E-10	-1.83041778891067E-10
a_{17}	2.70696987426965E-09	6.38633660881426E-10	1.13559401945631E-08	6.91210108611807E-09
a_{16}	-8.60726676073100E-08	-2.15860698170760E-08	-4.23443634996111E-07	-1.79421624357313E-07
a_{15}	1.99672241348144E-06	5.32014185913731E-07	1.14827197738592E-05	3.39554188811152E-06
a_{14}	-3.49671870813340E-05	-9.89258532039311E-06	-2.33996134704937E-04	-4.84964500451427E-05
a_{13}	4.71858227548241E-04	1.41658384951966E-04	3.65782932967479E-03	5.33923875125635E-04
a_{12}	-4.96490014850410E-03	-1.58072907656754E-03	-4.46159894598517E-02	-4.58990766259511E-03
a_{11}	4.09608635990690E-02	1.38220240165315E-02	4.35893173834714E-01	3.10299787267823E-02
a_{10}	-2.65085817034957E-01	-9.47553302295150E-02	-3.61601578812868E+00	-1.65442577025842E-01
a_9	1.34015337060141E+00	5.07212650697691E-01	2.83584401456879E+01	6.95224638185723E-01
a_8	-5.24610954865750E+00	-2.10176365496657E+00	-2.29949402031930E+02	-2.29393978205187E+00
a_7	1.56799510670546E+01	6.65060977606740E+00	1.84181273483385E+03	5.90167309055049E+00
a_6	-3.50645927689308E+01	-1.57588630366621E+01	-1.28544848134067E+04	-1.17086625574475E+01
a_5	5.70318262445195E+01	2.72187299544167E+01	7.12125711598618E+04	1.76155822073721E+01
a_4	-6.48907410098701E+01	-3.30491167052668E+01	-2.96796397060977E+05	-1.96096765470814E+01
a_3	4.90311187858117E+01	2.69490135500644E+01	8.90809205667305E+05	1.56667315641923E+01
a_2	-2.32888796937463E+01	-1.42413754887764E+01	-1.81382736757085E+06	-8.94579854442243E+00
a_1	7.50645624360757E+00	5.57583257139493E+00	2.24195271112227E+06	4.39804082518896E+00
a_0	5.17008262248863E-02	2.95257563410426E-01	-1.26991681840798E+06	-3.86012635387946E-01
dev_{max} (mm)	23.564E-03	26.289E-03	30.831E-03	6.276E-03
Range (mm)	0<z<16.26	0<z<17.44	0<z<13.23	0<z<13.63

Table. A.1 Interface data of clean and contaminated bubbles shown in Fig. 6 – continued

$$r_b(mm) = a_{20}z^{20} + a_{19}z^{19} + a_{18}z^{18} + a_{17}z^{17} + a_{16}z^{16} + a_{15}z^{15} + a_{14}z^{14} + a_{13}z^{13} + a_{12}z^{12} + a_{11}z^{11} + a_{10}z^{10} + a_9z^9 + a_8z^8 + a_7z^7 + a_6z^6 + a_5z^5 + a_4z^4 + a_3z^3 + a_2z^2 + a_1z + a_0$$

Fig. 6	c		d	
Coefficients	**clean**	**contaminated**	**clean**	**contaminated**
a_{20}	-9.28490938485168E-12	-1.01434328117774E-13	-1.96162564918123E-10	-7.23032707255770E-11
a_{19}	1.00692242595437E-09	1.24620892054285E-11	1.82684052225316E-08	6.86686903388259E-09
a_{18}	-5.06033666141633E-08	-6.76563459146997E-10	-7.88300582193555E-07	-3.02216313119092E-07
a_{17}	1.56394818289759E-06	2.07302351349529E-08	2.09162559550479E-05	8.18008849976712E-06
a_{16}	-3.32652617137538E-05	-3.61043613000415E-07	-3.81892777550636E-04	-1.52398024842053E-04
a_{15}	5.16347455517094E-04	2.09749846591526E-06	5.08765168945583E-03	2.07243070546108E-03
a_{14}	-6.05192200977038E-03	6.56245746026938E-05	-5.11707564690741E-02	-2.12876251631979E-02
a_{13}	5.46715009566159E-02	-2.21106341793525E-03	3.96604594913592E-01	1.68615130059554E-01
a_{12}	-3.85201204590206E-01	3.71138639933171E-02	-2.39687763388989E+00	-1.04232301917009E+00
a_{11}	2.12859710186701E+00	-4.23694974201007E-01	1.13572362526264E+01	5.05769951254364E+00
a_{10}	-9.22992028905145E+00	3.54870279481066E+00	-4.22092606750818E+01	-1.92788203159149E+01
a_9	3.12774973888715E+01	-2.23483617660009E+01	1.22521420077338E+02	5.75131801475940E+01
a_8	-8.21160662086720E+01	1.05946798054380E+02	-2.75312334622842E+02	-1.33189307460022E+02
a_7	1.64743190156590E+02	-3.70932254599017E+02	4.72236070737528E+02	2.36356660630884E+02
a_6	-2.47590830307266E+02	9.09877723052316E+02	-6.05993490012971E+02	-3.15545428113227E+02
a_5	2.71128456666118E+02	-1.33755962168544E+03	5.65802220024633E+02	3.09101449998095E+02
a_4	-2.08268420690747E+02	2.95062925783911E+02	-3.70140056760340E+02	-2.14998106797008E+02
a_3	1.06720705365266E+02	3.40608174007099E+03	1.61525294681252E+02	1.01960700300075E+02
a_2	-3.47140544416797E+01	-7.63980230100507E+03	-4.48383093533255E+01	-3.19005160104310E+01
a_1	8.07304594773088E+00	7.53855559015673E+03	8.93996280674196E+00	7.53987096238963E+00
a_0	1.29681757737575E-02	-3.01984486243346E+03	1.79899165500136E-01	6.59533685673801E-02
dev_{max} (mm)	8.990E-03	10.942E-03	9.516E-03	13.929E-03
Range (mm)	0<z<10.86	0<z<11.59	0<z<9.33	0<z<10.55

Notation

A	bubble surface area based on the bubble equivalent diameter
C^*	concentration of gas at interface
C	concentration of gas at the liquid bulk
Ca	Capillary number ($=\mu U_b/\sigma$)
C_L	water concentration
C_s	Concentration of surfactant at the liquid bulk
d	bubble diameter
d_{eq}	sphere-volume equivalent bubble diameter
D	channel hydraulic diameter
D_c	gas molecular diffusion coefficient
d_{max}	bubble diameter at its maximum cross section in the channel
dev_{max}	the maximum deviation in absolute distance between the interface sampling points extracted from the x-ray images and their nearest points on the fitted polynomial curve
E	radiographic extinction image
Eo	Eötvös number ($=\Delta\rho g D^2/\sigma$)

g	acceleration due to gravity
h	distance from the liquid surface
H	Henry's constant
I	X-ray intensity
k_L	liquid side mass transfer coefficient
k_La	liquid-phase volumetric mass transfer coefficient
k_s	calibration function
k_v	calibration function
La	Laplace number ($=C_s\beta/\alpha$)
L_b	bubble length
n	total moles of gas inside the bubble
P	pressure inside of the bubble
P_{atm}	atmospheric pressure
Pe	Peclet number ($=DU_b/D_c$)
r	radial direction, bubble radius
R	universal gas constant
Re	Reynolds number ($=\rho DU_b/\mu$)
S_e	surface coverage ratio
S_b	bubble's interfacial area
Sh	Sherwood number ($=Dk_L/D_c$)
t	time
T	bubble temperature
U_b	bubble terminal velocity
V_b	bubble volume
y	mole fraction of CO_2 inside of gas phase
z	axial direction
α	desorption rate constant
β	adsorption rate constant
ρ	liquid density
μ	liquid dynamic viscosity
μd	radiographic attenuation
σ	surface tension of liquid

References

[1] A. A. Donaldson, A. Macchi, and D. M. Kirpalani, "Predicting inter-phase mass transfer for idealized Taylor flow: A comparison of numerical frameworks," *Chem. Eng. Sci.*, vol. 66, no. 14, pp. 3339–3349, 2011.

[2] D. Bothe and J. Prüss, "Stability of equilibria for two-phase flows with soluble surfactant," *Q. J. Mech. Appl. Math.*, vol. 63, no. 2, pp. 177–199, 2010.

[3] M. E. Weber, "The effect of surface active agents on mass transfer from spherical cap bubbles," *Chem. Eng. Sci.*, vol. 30, no. 6, pp. 1507–1510, 1975.

[4] S. Sadhal and R. Johnson, "Stokes flow past bubbles and drops partially coated with thin films. Part 1. Stagnant cap of surfactant film- exact solution," *J. Fluid Mech.*, vol. 126, pp. 237–250, 1983.

[5] A. Dani, "Direct numerical simulation of mass transfer from spherical bubbles : the effect of interface contamination at low Reynolds numbers," *Int. J. Chem. React. Eng.*, vol. 4, pp. 1–21, 2006.

[6] M. Muradoglu and G. Tryggvason, “A front-tracking method for computation of interfacial flows with soluble surfactants,” *J. Comput. Phys.*, vol. 227, pp. 2238–2262, 2008.

[7] R. Clift, J. Grace, and M. Weber, *Bubbles, drops, and particles*, First ed. New York: Academic Press, 1978.

[8] S. Tasoglu, U. Demirci, and M. Muradoglu, “The effect of soluble surfactant on the transient motion of a buoyancy-driven bubble,” *Phys. Fluids*, vol. 20, no. 4, pp. 17–20, 2008.

[9] B. Cuenot, J. Magnaudet, and B. Spennato, “The effects of slightly soluble surfactants on the flow around a spherical bubble,” *J. Fluid Mech.*, vol. 339, pp. 25–53, 1997.

[10] K. Hayashi and A. Tomiyama, “Effects of surfactant on terminal velocity of a Taylor bubble in a vertical pipe,” *Int. J. Multiph. Flow*, vol. 39, pp. 78–87, 2012.

[11] S. N. Ghadiali and D. P. Gaver, “The influence of non-equilibrium surfactant dynamics on the flow of a semi-infinite bubble in a rigid cylindrical capillary tube,” *J. Fluid Mech.*, vol. 478, pp. 165–196, 2003.

[12] G. M. Ginley and C. J. Radke, “Influence of Soluble Surfactants on the Flow of Long Bubbles Through a Cylindrical Capillary,” *ACS Symp. Ser. 396*, pp. 480–501, 1989.

[13] J. Ratulowski and H.-C. Chang, “Marangoni effects of trace impurities on the motion of long gas bubbles in capillaries,” *J. Fluid Mech.*, vol. 210, pp. 303–328, 1990.

[14] K. J. Stebe and D. Barthès-Biesel, “Marangoni effects of adsorption-desorption controlled surfactants on the leading end of an infinitely long bubble in a capillary,” *J. Fluid Mech.*, vol. 286, pp. 25–48, 1995.

[15] C.-W. Park, “Influence of soluble surfactants on the motion of a finite bubble in a capillary tube,” *Phys. Fluids A Fluid Dyn.*, vol. 4, no. 11, pp. 2335–2347, 1992.

[16] P. Daripa and G. Pasa, “The effect of surfactant on long bubbles rising in vertical capillary tubes,” *J. Stat. Mech. Theory Exp.*, vol. 2011, no. 2, p. L02003, 2011.

[17] P. Daripa and G. Pasa, “The effect of surfactant on the motion of long bubbles in horizontal capillary tubes,” *J. Stat. Mech. Theory Exp.*, vol. 2010, no. 2, p. L02002, 2010.

[18] U. Olgac and M. Muradoglu, “Effects of surfactant on liquid film thickness in the Bretherton problem,” *Int. J. Multiph. Flow*, vol. 48, pp. 58–70, 2013.

[19] K. H. Mancy and D. A. Okun, “Effects of surface active agents on bubble aeration,” *Water Pollut. Control Fed.*, vol. 32, no. 4, pp. 351–364, 1960.

[20] R. M. Griffith, “The effect of surfactants on the terminal velocity of drops and bubbles,” *Chem. Eng. Sci.*, vol. 17, pp. 1057–1070, 1962.

[21] D. R. Raymond and S. A. Zieminski, “Mass transfer and drag coefficients of bubbles rising in dilute aqueous solutions,” *AIChE J.*, vol. 17, no. 1, pp. 57–65, 1971.

[22] G. Vázquez, M. a. Cancela, R. Varela, E. Alvarez, and J. M. Navaza, “Influence of surfactants on absorption of CO2 in a stirred tank with and without bubbling,” *Chem. Eng. J.*, vol. 67, no. 2, pp. 131–137, 1997.

[23] G. Vázquez, M. Cancela, C. Riverol, E. Alvarez, and J. Navaza, “Application of the Danckwerts method in a bubble column,” *Chem. Eng. J.*, vol. 78, no. 1, pp. 13–19, 2000.

[24] F. Takemura and A. Yabe, “Rising speed and dissolution rate of a carbon dioxide bubble in slightly contaminated water,” *J. Fluid Mech.*, vol. 378, pp. 319–334, Jan. 1999.

[25] J. M. T. Vasconcelos, J. M. L. Rodrigues, S. C. P. Orvalho, S. S. Alves, R. L. Mendes, and A. Reis, “Effect of contaminants on mass transfer coefficients in bubble column and airlift contactors,” *Chem. Eng. Sci.*, vol. 58, no. 8, pp. 1431–1440, 2003.

[26] K. Loubière and G. Hébrard, “Influence of liquid surface tension (surfactants) on bubble formation at rigid and flexible orifices,” *Chem. Eng. Process. Process Intensif.*, vol. 43, no. 11, pp. 1361–1369, 2004.

[27] S. S. Alves, S. P. Orvalho, and J. M. T. Vasconcelos, “Effect of bubble contamination on rise velocity and mass transfer,” *Chem. Eng. Sci.*, vol. 60, no. 1, pp. 1–9, 2005.

[28] S. S. Alves, C. I. Maia, and J. M. T. Vasconcelos, “Gas-liquid mass transfer coefficient in stirred tanks interpreted through bubble contamination kinetics,” *Chem. Eng. Process. Process Intensif.*, vol. 43, no. 7, pp. 823–830, 2004.

[29] E. Almatroushi and A. Borhan, “Surfactant effect on the buoyancy-driven motion of bubbles and drops in a tube,” *Ann. N. Y. Acad. Sci.*, vol. 1027, no. 1, pp. 330–341, 2004.

[30] P. Painmanakul, K. Loubière, G. Hébrard, M. Mietton-Peuchot, and M. Roustan, “Effect of surfactants on liquid-side mass transfer coefficients,” *Chem. Eng. Sci.*, vol. 60, no. 22, pp. 6480–6491, 2005.

[31] R. Sardeing, P. Painmanakul, and G. Hébrard, “Effect of surfactants on liquid-side mass transfer coefficients in gas–liquid systems: A first step to modeling ,” *Chem. Eng. Sci.* , vol. 61, no. 19, pp. 6249–6260, 2006.

[32] D. Rosso, D. L. Huo, and M. K. Stenstrom, “Effects of interfacial surfactant contamination on bubble gas transfer,” *Chem. Eng. Sci.*, vol. 61, no. 16, pp. 5500–5514, 2006.

[33] N. J. English and S. G. Kandlikar, “An experimental investigation into the effect of surfactants on air-water two-phase flow in minichannels,” *Heat Transf. Eng.*, vol. 27, no. 4, pp. 99–109, 2006.

[34] N. J. English and S. G. Kandlikar, “An experimental investigation into the effect of surfactants on air-water two-phase flow in minichannels,” in *3rd International Conference on Microchannels and Minichannels June Toronto, Canada*, 2005, pp. 1–10.

[35] S. Takagi, T. Ogasawara, M. Fukuta, and Y. Matsumoto, “Surfactant effect on the bubble motions and bubbly flow structures in a vertical channel,” *Fluid Dyn. Res.*, vol. 41, no. 6, p. 65003, 2009.

[36] G. Hebrard, J. Zeng, and K. Loubiere, “Effect of surfactants on liquid side mass transfer coefficients: A new insight,” *Chem. Eng. J.*, vol. 148, no. 1, pp. 132–138, 2009.

[37] M. Jamnongwong, K. Loubiere, N. Dietrich, and G. Hébrard, “Experimental study of oxygen

diffusion coefficients in clean water containing salt, glucose or surfactant: Consequences on the liquid-side mass transfer coefficients," *Chem. Eng. J.*, vol. 165, no. 3, pp. 758–768, 2010.

[38] S. Takagi and Y. Matsumoto, "Surfactant effects on bubble motion and bubbly flows," *Annu. Rev. Fluid Mech.*, vol. 43, no. 1, pp. 615–636, 2011.

[39] D. D. McClure, A. C. Lee, J. M. Kavanagh, D. F. Fletcher, and G. W. Barton, "Impact of surfactant addition on oxygen mass transfer in a bubble column," *Chem. Eng. Technol.*, vol. 38, no. 1, pp. 44–52, 2015.

[40] J. Huang and T. Saito, "Influence of bubble-surface contamination on instantaneous mass transfer," *Chem. Eng. Technol.*, vol. 38, no. 11, pp. 1947–1954, 2015.

[41] J. Aoki, K. Hayashi, and A. Tomiyama, "Mass transfer from single carbon dioxide bubbles in contaminated water in a vertical pipe ," *Int. J. Heat Mass Transf.* , vol. 83, no. 0, pp. 652–658, 2015.

[42] J. Aoki, K. Hayashi, S. Hosokawa, and A. Tomiyama, "Effects of surfactants on mass transfer from single carbon dioxide bubbles in vertical pipes," *Chem. Eng. Technol.*, vol. 38, no. 11, pp. 1955–1964, 2015.

[43] R. Krechetnikov and G. M. Homsy, "Experimental study of substrate roughness and surfactant effects on the Landau-Levich law," *Phys. Fluids*, vol. 17, no. 10, p. 102108, 2005.

[44] G. Schulze and E. U. Schlünder, "Physical absorption of single gas bubbles in degassed and preloaded water," *Chem. Eng. Process.*, vol. 19, no. 1, pp. 27–37, 1985.

[45] M. Haghnegahdar, S. Boden, and U. Hampel, "Investigation of mass transfer in milli-channels using high-resolution microfocus X-ray imaging," *Int. J. Heat Mass Transf.*, vol. 93, pp. 653–664, 2015.

[46] M. Haghnegahdar, S. Boden, and U. Hampel, "Mass transfer measurement in a square milli-channel and comparison with results from a circular channel," *Int. J. Heat Mass Transf.*, vol. 101, pp. 251–260, 2016.

[47] S. Hosoda, S. Abe, S. Hosokawa, and A. Tomiyama, "Mass transfer from a bubble in a vertical pipe," *Int. J. Heat Mass Transf.*, vol. 69, pp. 215–222, 2014.

[48] E. T. White and R. H. Beardmore, "The velocity of rise of single cylindrical air bubbles through liquids contained in vertical tubes," *Chem. Eng. Sci.*, vol. 17, no. 5, pp. 351–361, 1962.

[49] R. Kurimoto, K. Hayashi, and A. Tomiyama, "Terminal velocities of clean and fully-contaminated drops in vertical pipes," *Int. J. Multiph. Flow*, vol. 49, pp. 8–23, 2013.

[50] F. P. Bretherton, "The motion of long bubbles in tubes," *J. Fluid Mech.*, vol. 10, pp. 166–188, 1961.

[51] P. Daripa and G. Paşa, "The thickening effect of interfacial surfactant in the drag-out coating problem," *J. Stat. Mech. Theory Exp.*, vol. 2009, no. 7, p. L07002, 2009.

[52] T. N. Swaminathan, K. Mukundakrishnan, P. S. Ayyaswamy, and D. M. Eckmann, "Effect of a soluble surfactant on a finite sized bubble motion in a blood vessel," *J. Fluid Mech.*, vol. 642,

pp. 509–539, 2010.

[53] A. Q. Shen, B. Gleason, G. H. McKinley, and H. a. Stone, “Fiber coating with surfactant solutions,” *Phys. Fluids*, vol. 14, no. 11, pp. 4055–4068, 2002.

[54] L.-H. Chen and Y.-L. Lee, “Adsorption behavior of surfactants and mass transfer in single-drop extraction,” *AIChE J.*, vol. 46, no. 1, pp. 160–168, 2000.

[55] Y. L. Lee, “Surfactants effects on mass transfer during drop-formation and drop falling stages,” *AIChE J.*, vol. 49, no. 7, pp. 1859–1869, 2003.

[56] R. M. Griffith, “Mass transfer from drops and bubbles,” *Chem. Eng. Sci.*, vol. 12, no. 3, pp. 198–213, 1960.

[57] J. M. T. Vasconcelos, S. P. Orvalho, and S. S. Alves, “Gas–liquid mass transfer to single bubbles: Effect of surface contamination,” *AIChE J.*, vol. 48, no. 6, pp. 1145–1154, 2002.

[58] S. Y. Lin, K. McKeigue, and C. Maldarelli, “Diffusion controlled surfactant adsorption studied by pendant drop digitisation,” vol. 36, no. 12, pp. 1785–1795, 1990.

[59] K. J. Stebe, S. Y. Lin, and C. Maldarelli, “Remobilizing Surfactant Retarded Fluid Particle Interfaces .1. Stress-Free Conditions at the Interfaces of Micellar Solutions of Surfactants with Fast Sorption Kinetics,” *Phys. Fluids A-Fluid Dyn.*, vol. 3, no. 1991, pp. 3–20, 1991.

[60] K. J. Stebe and C. Maldarelli, “Remobilizing Surfactant Retarded Fluid Particle Interfaces,” *J. Colloid Interface Sci.*, vol. 163, no. 1, pp. 177–189, 1994.